Journal of Biomedical Optics

SPIEDigitalLibrary.org/jbo

Assessment of the effects of ultrasound-mediated glucose on permeability of normal, benign, and cancerous human lung tissues with the Fourier-domain optical coherence tomography

Huajiang Wei
Guoyong Wu
Zhouyi Guo
Hongqin Yang
Yonghong He
Shusen Xie
Xiao Guo

SPIE

Assessment of the effects of ultrasound-mediated glucose on permeability of normal, benign, and cancerous human lung tissues with the Fourier-domain optical coherence tomography

Huajiang Wei,[a] Guoyong Wu,[b] Zhouyi Guo,[a] Hongqin Yang,[c] Yonghong He,[d] Shusen Xie,[c] and Xiao Guo[a]
[a]South China Normal University, College of Biophotonics, MOE Key Laboratory of Laser Life Science & Institute of Laser Life Science, Guangzhou 510631, Guangdong Province, China
[b]Sun Yat-Sen University, First Affiliated Hospital, Department of Surgery, Guangzhou 510080, Guangdong Province, China
[c]Fujian Normal University, Key Laboratory of Optoelectronic Science and Technology for Medicine of Ministry of Education of China, Fuzhou 350007, Fujian, China
[d]Tsinghua University, Graduate School at Shenzhen, Shenzhen 518055, Guangdong, China

Abstract. The objective of this study was to evaluate the effects of ultrasound-mediated analyte diffusion on permeability of normal, benign, and cancerous human lung tissue *in vitro* and to find more effective sonophoretic (SP) delivery in combination with the optical clearing agents (OCAs) method to distinguish normal and diseased lung tissues. The permeability coefficients of SP in combination with OCAs diffusion in lung tissue were measured with Fourier-domain optical coherence tomography (FD-OCT). 30% glucose and SP with a frequency of 1 MHz and an intensity of 0.80 W/cm^2 over a 3 cm probe was simultaneously applied for 15 min. Experimental results show that the mean permeability coefficients of 30% glucose/SP were found to be $(2.01 \pm 0.21) \times 10^{-5}$ cm/s from normal lung (NL) tissue, $(2.75 \pm 0.28) \times 10^{-5}$ cm/s from lung benign granulomatosis (LBG) tissue, $(4.53 \pm 0.49) \times 10^{-5}$ cm/s from lung adenocarcinoma tumor (LAT) tissue, and $(5.81 \pm 0.62) \times 10^{-5}$ cm/s from lung squamous cell carcinoma (LSCC) tissue, respectively. The permeability coefficients of 30% glucose/SP increase approximately 36.8%, 125.4%, and 189.1% for the LBG, LAT, and LSCC tissue compared with that for the NL tissue, respectively. There were statistically significant differences in permeability coefficients of 30% glucose/SP between LBG and NL tissue ($p < 0.05$), between LAT and NL tissue ($p < 0.05$), and between LSCC and NL tissue ($p < 0.05$). The results suggest that the OCT functional imaging technique to combine an ultrasound-OCAs combination method could become a powerful tool in early diagnosis and monitoring of changed microstructure of pathologic human lung tissue. [DOI: 10.1117/1.JBO.17.11.116006]

Keywords: lung cancer; ultrasound; glucose; permeability coefficient; Fourier-domain optical coherence tomography.

Paper 12313 received May 22, 2012; revised manuscript received Oct. 2, 2012; accepted for publication Oct. 3, 2012; published online Nov. 1, 2012.

1 Introduction

Lung cancer is the leading cause of cancer-related mortality worldwide, with nearly 1.4 million deaths each year.[1–3] Lung cancer is diagnosed at an advanced stage in a majority of patients, which is the primary reason behind the high mortality rate associated with this disease. Early detection continues to be an elusive goal, and substantial numbers of patients diagnosed with localized disease are often unsuitable for curative surgical procedures due to concomitant medical illness. Non-small cell lung cancer (NSCLC), which includes adenocarcinoma, squamous cell carcinoma, large cell carcinoma, and bronchioloalveolar carcinoma, accounts for nearly 85% of all cases of lung cancer.[2,3] Cigarette smoking is the most common etiological factor, accounting for nearly 85% of patients with lung cancer.[2,3]

White light reflectance (WLR) color imaging endoscopy is the standard for clinical detection and localization of lung cancer. However, it suffers from poor sensitivity for early cancer detection. The diagnostic sensitivity of WLR imaging for early lung cancer is only about 9%.[4] Preinvasive lesions such as carcinoma *in situ* (CIS) and moderate or severe dysplasia are only a few cell layers thick and may not show enough morphological changes or color variations detectable by a WLR image. As a scattering medium, tissue shows optical effects that are characteristic of turbid physical systems.[5] Much of the light scattering in biological tissues is due to variations in polarizability, which can be characterized by variations in the index of refraction.

In addition, the shape, size, and distribution of tissue constituents play an important role in the overall scattering properties of tissue.[6] The refractive index mismatch of biological tissue components as a highly scattering medium has a strong influence on optical transmittance and reflectance, as well as on polarization and coherence of the scattered light.[7] Light-based therapeutic and diagnostic techniques could be improved if scattering within tissue were temporarily reduced. Laser surgery and therapy would benefit from the increased depth of penetration. Imaging modalities, such as fluorescence

Address all correspondence to: Huajiang Wei, South China Normal University, College of Biophotonics, MOE Key Laboratory of Laser Life Science & Institute of Laser Life Science, Guangzhou 510631, Guangdong Province, China. Tel: 86-020-85217070; Fax: 86-020-85216052; E-mail: weihj@scnu.edu.cn

0091-3286/2012/$25.00 © 2012 SPIE

microscopy, confocal imaging, and optical coherence tomography (OCT), would also benefit from an increased penetration depth.[6] It is well known that the turbidity of a dispersive physical system can be effectively controlled using an immersion effect (matching the refractive indices of scatterers and the base material) as well as by changes in the size of scatterers and their packing (the volumetric arrangement affects the spatial correlation of the scatterers).[5] The optical (scattering) properties of living tissue can be controlled by using various physical and chemical reactions such as compression, stretching, dehydration, coagulation, ultraviolet (UV) irradiation, low-temperature application (reversible cold cataract), and addition of chemicals.[5,8–13]

Several recent studies have demonstrated that sonophoretic (SP) delivery, as a noninvasive physical method, exhibited an enhanced tissue-clearing effect when applied topically with optical clearing agents (OCAs).[14–17] The significant ultrasound-induced enhancement in OCT imaging depth and contrast of *in vitro* porcine skin and *in vivo* human skin was found.[18,19] Several imaging techniques have been used to study the permeation of analytes in biological tissues,[20] including ultrasound,[21] magnetic resonance imaging (MRI),[22] optical projection tomography (OPT),[23] and OCT.[24–28] OCT is particularly attractive because it is a nondestructive, noninvasive technique that provides high-resolution, real-time images of biological tissues. OCT has been used extensively in tissue studies[24–28] to measure permeation of different molecules and materials through various epithelial tissues, such as rabbit sclera,[25] monkey skin,[26] rabbit cornea,[27] porcine aorta,[26,28] human skin,[29] and human esophagus.[30]

Ultrasound-mediated bioeffects are generally believed to be caused by cavitation.[31] Acoustic cavitation involves the creation and oscillation of gas bubbles in a liquid.[32] Cavitation bubbles may exhibit sustained growth and oscillations over several acoustic cycles (stable cavitation) or violent growth and collapse in less than a cycle (transient or inertial cavitation).[32] Potentially, both stable and transient cavitation may induce membrane permeabilization.[33] A large number of studies have reported on the SP delivery of small molecules through the skin in transdermal drug delivery (TDD).[34] It represents a useful noninvasive physical method to enhance epidermal permeability. In spite of the wide use of SP delivery in TDD, there are few studies to develop SP delivery for the effects of glucose permeability of normal, benign, and cancerous human lung tissues. The objectives of our study were to evaluate the effects of glucose mediated with ultrasound on permeability of normal, benign, and cancerous human lung tissue, to monitor and quantify the differences in permeability coefficients of ultrasound-OCAs combination in human normal lung (NL), lung benign granulomatosis (LBG), lung adenocarcinoma tumor (LAT), and lung squamous cell carcinoma (LSCC) tissue *in vitro* by the Fourier-domain optical coherence tomography (FD-OCT).

2 Materials and Methods

2.1 *Tissue Preparation*

A total of 48 samples of surgically resected human lung tissues were obtained from patients whose consents were obtained for the study at the First Affiliated Hospital of Sun Yat-Sen University. The samples were divided into four groups according to histological diagnosis: NL tissue (12 samples), LBG tissue (12 samples), LSCC tissue (12 samples), and LAT tissue (12 samples). Each removed tissue section was stored in 0.9% sodium chloride solution as soon as possible after the resection and then placed on ice and transported to the laboratory for performing measurements. They were stored at −70°C until the measurement *in vitro*. Each tissue was cut into an approximately 3.2×3.2 cm piece and placed into physiological saline solution for each OCT measurement.

2.2 *OCT System*

The experiments were performed by using an FD-OCT system. It is made by Shenzhen MOPTIM Imaging Technique Co., Ltd., China. A schematic of the OCT system was shown in the literature.[35] The optical source used in this system is a low-coherence broadband superluminescent diode with a wavelength of 830 ± 40 nm and an output power of 5 mW. The FD-OCT system provides an axial resolution of 12 μm and a transverse resolution of 15 μm in free space, determined by the focal spot size of the probe beam. The signal-to-noise ratio of the OCT system is measured to be 120 dB. 2-D images are obtained by scanning the incident beam over the sample surface in the lateral direction and in-depth (A-scan) scanning by the interferometer. The acquisition time per OCT image is about 180 ms, corresponding to an A-scan frequency of 2000 Hz. A computer is used to control the OCT system with a data acquisition software written in LabVIEW 7.2-D. OCT images obtained in the experiment were stored in the computer for further processing.

2.3 *Ultrasound and Glucose Application*

A DM-F608 sonicator with a 3-cm-diameter probe (Dimyth Beauty Equipment Manufacture, Guangzhou, China) was used for ultrasound application. The ultrasound frequency and intensity were 1 to 1.1 MHz and 0.80 W/cm^2, respectively. Sonicators with the frequency are most commonly used in cosmetic treatments and TDD.

Glucose was purchased from the Tianjin Damao Chemical Reagent Factory (Tianjin, China). The concentration of the glucose solutions used in this study was 30% (w/v) glucose solution. Solution of 30% (w/v) glucose was applied to the surface of each tissue of four different lung tissue types, and ultrasound were simultaneously performed on these samples for a period of 15 min, respectively. After 15 min of ultrasound treatment, a small amount of 30% glucose solution was discontinuously added to the surface of the samples for a total 120 min at a time interval of 30 min, respectively. At 0 min, these lung samples treated with glucose/SP are native. For the first 15 min of treatment, the samples with glucose/SP were applied with the ultrasound, while the samples of four different control groups were only applied with glucose for the whole 120 min. During the ultrasound treatment, the ultrasound probe was immersed in 30% glucose solution that was topically applied to the surface of tissue.

2.4 *OCT Measurements*

OCT images were continuously acquired from each lung sample for about 120 min. Right before the OCT experiments, the tissues were left under room temperature for 30 min. The lung sections were kept moist by phosphate-buffered saline to avoid dehydration and the optical probe was never in contact with the sample during the scanning process. The position of the probe beam on the scanned tissue was monitored using a visible light guiding beam. The selected region of the samples was

imaged for about 8 to 10 min before the addition of 30% glucose/SP to record a baseline, and then 30% glucose/SP was applied to the surface of lung specimens for a period of 15 min. The solutions were removed prior to OCT imaging. Every 30 min during the measurement, glucose solution was applied again on the tissue for 5 min. Then the OCT imaging was continuously monitored for about 2 h, and the room temperature was maintained at 22°C throughout the entire experiment. No tissues were used in more than one experiment.

2.5 *Data Processing*

In this study, OCT images obtained from lung tissue were processed using an original program developed in the MATLAB program to obtain the OCT signal and calculate the OCT signal slope (OCTSS). The OCTSS method has already been explained in detail in Refs. 24 to 30. The design of the system has been described by us previously.[29,30,36]

With the OCTSS method, the mean permeability coefficient of a specific region in the lung tissue was calculated by analyzing the slope changes in the OCT signal caused by 30% glucose/SP. 2-D OCT images were averaged laterally (approximately over 1 mm, which was enough for speckle noise suppression), and a single 1-D curve was produced that represented the measurement of the OCT signal in the sample on a logarithmic scale. As noise is inevitable in the measurement, a best-fit exponential curve is applied to the averaged 1-D OCT signal profile of each group. A region in the 1-D OCT signal was chosen where the signal was linear and underwent minimal alterations, and its thickness z_{region} was measured. Slopes of five consecutive OCT signals were averaged in this paper, normalized and plotted as a function of time.

The local increase of glucose concentration in the chosen region caused the scattering coefficient to decrease, which was clearly reflected in the OCTSS graph.[37] The time t_{region} was calculated by measuring from the point where the OCTSS started to decrease to the point at which a change in the slope of the OCT signal indicated that the diffusion had ended and the reverse process began to take place. An increase of the local glucose concentration induced a decrease of the OCT signal slope. The reverse process, designated by the positive slope change, is thought to have stemmed from the difference in the concentration gradients on both sides of the tissue causing the fluid to travel from the region of higher concentration to the lower one water reentering the tissue after diffusing out due to the application of glucose. The permeability coefficient P was then calculated by dividing the thickness of the region selected by the time it took for glucose to diffuse through in Eq. (1):[24–30,38]

$$\bar{P} = \frac{z_{\text{region}}}{t_{\text{region}}}. \tag{1}$$

2.6 *Statistical Analysis*

The data from all samples were presented as means ± SD and analyzed by an SPSS 10.0 software paired-test. The $p < 0.05$ value indicated significant difference.

3 Results and Discussion

In this investigation, the main purpose of this pilot study was to evaluate the effects of ultrasound-mediated glucose on permeability of normal, benign, and cancerous human lung tissues, to monitor and quantify the differences in permeability coefficients of ultrasound-OCAs combination in four different kinds of lung tissue by the FD-OCT, and to find a more effective ultrasound-OCAs combination method to distinguish normal and diseased human lung tissues than pure OCAs.

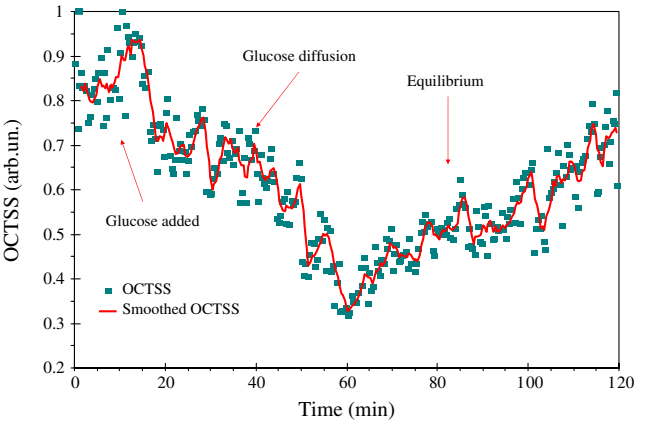

Fig. 1 OCT signal slope as a function of time recorded from NL tissue treatment with 30% glucose and ultrasound.

The OCTSS of four kinds of lung tissue were calculated from the 80 μm region at a tissue depth of approximately 230 μm from the tissue surface. The OCTSS graphs were analyzed to obtain the permeability coefficients. First, the lung tissue was imaged for about 10 min to record the OCTSS base line as a control OCTSS with no glucose/SP added. During this time, the time series of OCTSS fluctuation was induced by the sample (NL, LBG, LAT, and LSCC tissue) scanning as shown in Figs. 1, 2, 3, and 4. After the 10 min period, 30% glucose/SP was topically applied to the OCT scanning area where imaging continued for another 2 h. Figure 1 displays a typical OCTSS graph as a function of time for NL tissue with the topical application of 30% glucose/SP. Diffusion of ultrasound-mediated glucose solution inside the lung tissues dynamically changed the local scattering coefficient and it was detected by the OCT system. The OCTSS decreased due to the reduction of scattering inside the tissue caused by the local increase of glucose concentration, and decrease of water content in the interstitial space due to osmotic action of glucose.[24,25,27] The increase in slope at the

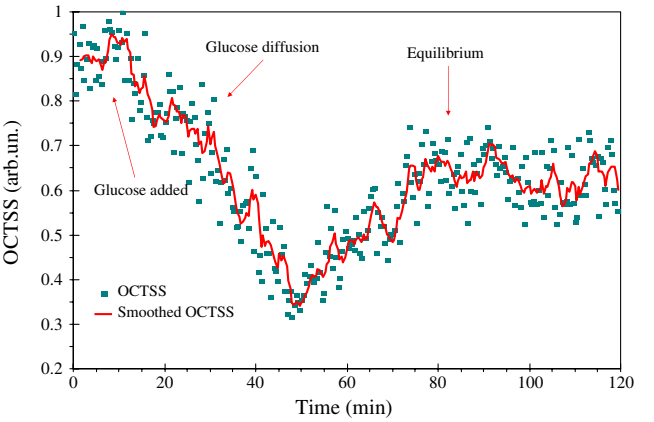

Fig. 2 OCT signal slope as a function of time recorded from LBG tissue treatment with 30% glucose and ultrasound.

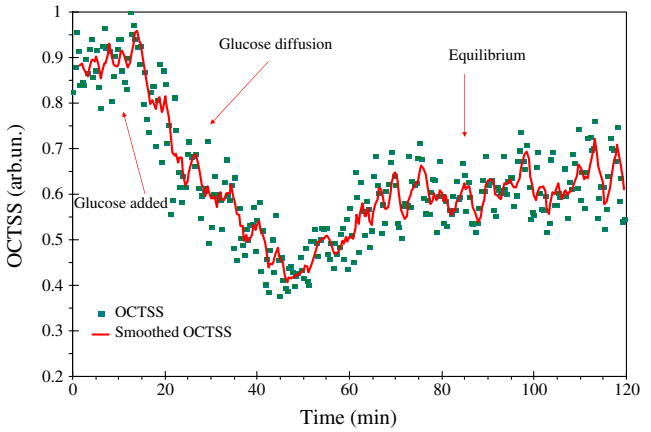

Fig. 3 OCT signal slope as a function of time recorded from LAT tissue treatment with 30% glucose and ultrasound.

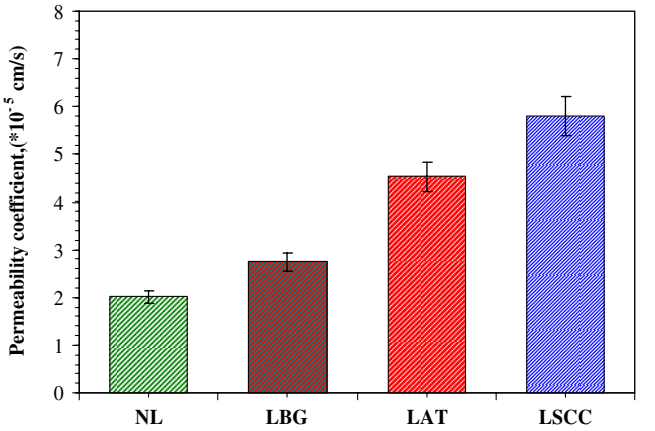

Fig. 5 Comparing permeability coefficients of 30% glucose/SP diffusion in NL, LBG, LAT, and LSCC tissue *in vitro*.

end of the graph is thought to be the reverse process. Water starts to diffuse into the tissue due to the difference in concentration created by the increase of glucose concentration.

In Fig. 1, the diffusion of glucose solution at NL tissue took approximately 52 min to reach an equilibrium state. A smoothed time-signal was obtained by adjacent averaging every five points. The mean permeability coefficient of 30% glucose/SP in NL tissue was measured in 12 independent experiments, which was estimated to be $(2.01 \pm 0.21) \times 10^{-5}$ cm/s cm/s. Similarly, Figs. 2, 3, and 4 show the OCTSS graphs as a function of time for LBG, LAT, and LSCC tissue with the topical application of 30% glucose/SP, respectively. The changing trends in the OCTSS of LBG, LAT, and LSCC tissue are also similar to that of NL tissues. In Figs. 2, 3, and 4, the diffusion of glucose solution at LBG, LAT, and LSCC tissue took approximately 40, 37, and 31 min to reach an equilibrium state, respectively. Their mean permeability coefficients of 30% glucose/SP were $(2.75 \pm 0.28) \times 10^{-5}$, $(4.53 \pm 0.49) \times 10^{-5}$, and $(5.81 \pm 0.62) \times 10^{-5}$ cm/s, respectively.

Figure 5 represents the comparison of permeability coefficients for four different types of lung tissues with the topical application of 30% glucose/SP *in vitro*. The results shown in Fig. 5 illustrate that the permeability coefficients of 30% glucose/SP increase approximately 36.8%, 125.4%, and 189.1% for the LBG, LAT, and LSCC tissue compared with that for the NL tissue, respectively. There were statistically significant differences in permeability coefficients of 30% glucose/SP between LBG and NL tissue ($p < 0.05$), between LAT and NL tissue ($p < 0.05$), and between LSCC and NL tissue ($p < 0.05$).

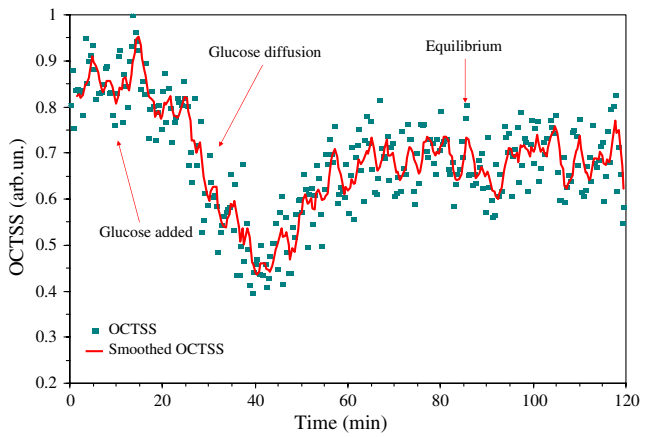

Fig. 4 OCT signal slope as a function of time recorded from LSCC tissue treatment with 30% glucose and ultrasound.

In our previous studies[35] the mean permeability coefficients have been reported for pure 30% glucose solution in human NL, LBG, LAT, and LSCC tissue *in vitro*. Comparison of the results of the current study with our previous studies[35] shows a significant increase in the permeability coefficients of 30% glucose/SP compared with that of pure 30% glucose in the NL, LBG, LAT, and LSCC tissue *in vitro*, respectively. Their increments are 48.9%, 54.5%, 57.3%, and 64.6%, respectively. This phenomenon is consistent with our previous findings that ultrasound caused the increase in permeability of normal breast and breast cancer tissue[17] and that ultrasound caused the increase of cell membrane permeability in TDD.[39–42] The studies have demonstrated the ultrasound-induced tissue optical clearing enhancement with topical application of 30% glucose on *in vitro* normal, benign, and malignant human lung. Moreover, their optical clearing effects are significantly different. In the last decade, many studies analyzed the relationship between tissue composition, microstructure, and macrophysiology, showing that the lung's physiological behavior reflects both the mechanical properties of tissue individual components and its complex structural organization.

Different lung pathologies can affect the extracellular matrix (ECM).[43] For example, the increased deposition of ECM proteins and fibroblasts in the stroma surrounding the epithelial cells of the breast is the leading risk factor for breast carcinoma (which accounts for 30% of breast cancer).[44] This and many other diseases might potentially be diagnosed by comparing the permeability rates of several therapeutic or diagnostic agents in normal and abnormal tissues.[26] Therefore, precise assessment of the diffusion processes in normal and abnormal tissues with OCT might provide a truly noninvasive way for evaluation of tissue health.[28] As yet, however, no published reports have demonstrated the capability of the OCT technique for quantifying the permeability coefficients of the ultrasound-OCAs combination in normal, benign, and malignant human lung tissue. Our experiment is the first reported investigation of ultrasound-mediated glucose diffusion in normal, benign, and malignant human lung tissue.

In our pilot experiments, the ultrasound was selected to enhance the glucose diffusion due to several reasons. First, the technique is noninvasive. Second, no insertion or surgery is needed, and acoustic transducers are placed in contact with the mixed solution that is spread on the tissue. Third, the method is extremely simple to implement (sonicators have been used in beauty parlors and clinics). Additionally, the cost is low. Ultrasound has demonstrated an enhanced transdermal mass transport effect when applied topically in TDD. Its mechanism is believed to be through acoustic cavitation, which is the formation and collapse of gaseous cavities, and has the dominant role in sonophoresis.[45,46] Based on the aforementioned results, it indicated that due to the ultrasound penetration enhancing and convection effect, more glucose can penetrate the lung tissue and glucose can penetrate more quickly to achieve more refractive index matching in human lung tissue *in vitro* to improve lung tissue optical clearing.

4 Conclusions

Our results demonstrate that simultaneous application of ultrasound and glucose led to a marked increase in the permeability coefficients for four different types of lung tissues *in vitro*. The permeability coefficients of 30% glucose/SP increase approximately 36.8%, 125.4%, and 189.1% for the LBG, LAT, and LSCC tissue compared with that for the NL tissue, respectively. The coadministration of OCAs diffusion under ultrasound-assistance is a more effective approach in using OCT imaging to diagnose normal, benign, and cancerous human lung tissues than that of pure OCAs.[35]

Acknowledgments

This work was supported by the National Natural Science Foundation of China (Grant Nos. 60778047 and 61275187), Specialized Research Fund for the Doctoral Program of Higher Education of China (Grant No. 20114407110001), the Natural Science Foundation of Guangdong Province of China (Grant Nos. 06025080 and 9251063101000009), the Key Science and Technology Project of Guangdong Province of China (Grant Nos. 2005B50101015 and 2008B090500125), the Key Science and Technology Project of Guangzhou City of China (Grant No. 2008Z1-D391), and Key Laboratory of Optoelectronic Science and Technology for Medicine (Fujian Normal University), Ministry of Education, China (Grant No. JYG1202).

References

1. A. Jemal et al., "Global patterns of cancer incidence and mortality rates and trends," *Cancer Epidemiol. Biomarkers Prev.* **19**(8), 1893–1907 (2010).
2. S. S. Ramalingam, T. K. Owonikoko, and F. R. Khuri, "Lung cancer: new biological insights and recent therapeutic advances," *CA Cancer J. Clin.* **61**(2), 91–112 (2011).
3. A. Hurria and M. G. Kris, "Management of lung cancer in older adults," *CA Cancer J. Clin.* **53**(6), 325–341 (2003).
4. S. Lam et al., "Localization of bronchial intraepithelial neoplastic lesions by fluorescence bronchoscopy," *Chest* **113**(3), 696–702 (1998).
5. V. V. Tuchin et al., "Light propagation in tissues with controlled optical properties," *J. Biomed. Opt.* **2**(4), 401–417 (1997).
6. G. Vargas et al., "Use of an agent to reduce scattering in skin," *Lasers Surg. Med.* **24**(2), 133–141 (1999).
7. V. V. Tuchin, "Optical immersion as a new tool for controlling the optical properties of tissues and blood," *Laser Phys.* **15**(8), 1109–1136 (2005).
8. V. V. Tuchin, "Laser light scattering in biomedical diagnostics and therapy," *J. Laser Appl.* **5**(2–3), 43–60 (1993).
9. B. Chance et al., "Effects of solutes on optical properties of biological materials: models, cells, and tissues," *Anal. Biochem.* **227**(2), 351–362 (1995).
10. H. Liu et al., "Dependence of tissue optical properties on solute-induced changes in refractive index and osmolarity," *J. Biomed. Opt.* **1**(2), 200–211 (1996).
11. V. V. Tuchin et al., "Optical and osmotic properties of human sclera," *Proc. SPIE* **2979**, 658–675 (1997).
12. J. S. Maier et al., "Possible correlation between blood glucose concentration and the reduced scattering coefficient of tissues in the near infrared," *Opt. Lett.* **19**(24), 2062–2064 (1994).
13. M. Kohl et al., "Influence of glucose concentration on light scattering in tissue-simulating phantoms," *Opt. Lett.* **19**(24), 2170–2172 (1994).
14. X. Q. Xu, Q. H. Zhu, and C. J. Sun, "Assessment of the effects of ultrasound-mediated alcohols on skin optical clearing," *J. Biomed. Opt.* **14**(3), 034042 (2009).
15. C. Y. Huang, B. Liu, and M. E. Brezinski, "Ultrasound-enhanced optical coherence tomography: improved penetration and resolution," *J. Opt. Soc. Am. A* **25**(4), 938–946 (2008).
16. H. Q. Zhong et al., "*In vitro* study of ultrasound and different-concentration glycerol—induced changes in human skin optical attenuation assessed with optical coherence tomography," *J. Biomed. Opt.* **15**(3), 036012 (2010).
17. H. Q. Zhong et al., "Enhancement of permeability of glycerol with ultrasound in human normal and cancer breast tissues in vitro using optical coherence tomography," *Laser Phys. Lett.* **7**(5), 388–395 (2010).
18. X. Xu and Q. Zhu, "Feasibility of sonophoretic delivery for effective skin optical clearing," *IEEE Biomed. Eng.* **55**(4), 1432–1437 (2008).
19. X. Xu and Q. Zhu, "Sonophoretic delivery for contrast and depth improvement in skin optical coherence tomography," *IEEE J. Sel. Topics Quantum Electron.* **14**(1), 56–61 (2008).
20. M. G. Ghosn et al., "Permeation of human plasma lipoproteins in human carotid endarterectomy tissues: measurement by optical coherence tomography," *J. Lipid Res.* **52**(7), 1429–1434 (2011).
21. B. B. Goldberg, "Ultrasound contrast agents," *Clin. Diagn. Ultrasound* **28**, 35–45 (1993).
22. H. Uematsu et al., "Vascular permeability: quantitative measurement with double-echo dynamic MR imaging—theory and clinical application," *Radiology* **214**(3), 912–917 (2000).
23. J. Ripoll, H. Meyer, and A. Garofalakis, "*In vivo* optical tomography: from diffusion to ballistic," *Opt. Mater.* **31**(7), 1082–1085 (2009).
24. K. V. Larin and V. V. Tuchin, "Functional imaging and assessment of the glucose diffusion rate in epithelial tissues in optical coherence tomography," *Quantum Electron.* **38**(6), 551–556 (2008).
25. M. G. Ghosn et al., "Differential permeability rate and percent clearing of glucose in different regions in rabbit sclera," *J. Biomed. Opt.* **13**(2), 021110 (2008).
26. M. G. Ghosn et al., "Monitoring of glucose permeability in monkey skin in vivo using optical coherence tomography," *J. Biophotonics* **3**(1–2), 25–33 (2010).
27. M. G. Ghosn, V. V. Tuchin, and K. V. Larin, "Nondestructive quantification of analyte diffusion in cornea and sclera using optical coherence tomography," *Invest. Ophthalmol. Visual Sci.* **48**(6), 2726–2733 (2007).
28. M. G. Ghosn et al., "Effect of temperature on permeation of low-density lipoprotein particles through human carotid artery tissues," *J. Biophotonics* **2**(10), 573–580 (2009).
29. X. Guo et al., "*In vivo* comparison of the optical clearing efficacy of optical clearing agents in human skin by quantifying permeability using optical coherence tomography," *Photochem. Photobiol.* **87**(3), 734–740 (2011).
30. Q. L. Zhao et al., "Quantifying glucose permeability and enhanced light penetration in *ex vivo* human normal and cancerous esophagus tissues with optical coherence tomography," *Laser Phys. Lett.* **8**(1), 71–77 (2011).
31. M. W. Miller, D. L. Miller, and A. A. Brayman, "A review of *in vitro* bioeffects of inertial ultrasonic from a mechanistic perspective," *Ultrasound Med. Biol.* **22**(9), 1131–1154 (1996).
32. T. Leighton, *The Acoustic Bubble*, Academic Press, San Diego (1997).
33. J. Sundaram, B. R. Mellein, and S. Mitragotri, "An experimental and theoretical analysis of ultrasound-induced permeabilization of cell membranes," *Biophys. J.* **84**(5), 3087–3101 (2003).

34. N. B. Smith, "Perspectives on transdermal ultrasound mediated drug delivery," *Int. J. Nanomedicine* **2**(4), 585–594 (2007).
35. X. Guo et al., "Quantification of glucose diffusion in human lung tissues by using Fourier domain optical coherence tomography," *Photochem. Photobiol.* **88**(2), 311–316 (2012).
36. X. Guo et al., "*In vivo* quantification of propylene glycol, glucose and glycerol diffusion in human skin with optical coherence tomography," *Laser Phys.* **20**(9), 1849–1855 (2010).
37. I. V. Larina et al., "Enhanced OCT imaging of embryonic tissue with optical clearing," *Laser Phys. Lett.* **5**(6), 476–479 (2008).
38. X. Q. Xu, Q. H. Zhu, and C. J. Sun, "Combined effect of ultrasound-SLS on skin optical clearing," *IEEE Photon. Technol. Lett.* **20**(24), 2117–2119 (2008).
39. G. A. Husseini and W. G. Pitt, "Ultrasonic-activated micellar drug delivery for cancer treatment," *J. Pharm. Sci.* **98**(3), 795–811 (2009).
40. K. Tachibana et al., "Enhanced cytotoxic effect of Ara-C by low intensity ultrasound to HL-60 cells," *Cancer Lett.* **149**(1–2), 189–194 (2000).
41. K. Tachibana et al., "Induction of cell-membrane porosity by ultrasound," *Lancet* **353**(9162), 1409 (1999).
42. S. Mitragotri and J. Kost, "Low-frequency sonophoresis: a noninvasive method of drug delivery and diagnostics," *Biotechnol. Prog.* **16**(3), 488–492 (2000).
43. D. S. Faffe and W. A. Zin, "Lung parenchymal mechanics in health and disease," *Physiol. Rev.* **89**(3), 759–775 (2009).
44. N. F. Boyd et al., "Mammographic densities and breast cancer risk," *Cancer Epidemiol. Biomarkers Prev.* **7**(12), 1133–1144 (1998).
45. S. Mitragotri, "Sonophoresis: a 50-year journey," *Drug Discov. Today* **9**(17), 735–736 (2004).
46. J. Sundaram, B. R. Mellein, and S. Mitragotri, "An experimental and theoretical analysis of ultrasound-induced permeabilization of cell membranes," *Biophys. J.* **84**(5), 3087–3101 (2003).